ACS Energy LETTERS

http://pubs.acs.org/journal/aelccp

Triboelectrification: Backflow and Stuck Charges Are Key

Hyunseok Ko,[‖] Yeong-won Lim,[‖] Seungwu Han, Chang Kyu Jeong,* and Sung Beom Cho*

Cite This: *ACS Energy Lett.* 2021, 6, 2792−2799

Read Online

ACCESS | Metrics & More | Article Recommendations | Supporting Information

ABSTRACT: To understand the most intrinsic mechanism of triboelectrification (TE), a straightforward framework of TE between metal and single-crystal dielectrics is designed by utilizing both experiments and first-principles calculations. Various theoretical models on charge transfer are examined with first-principles calculations. Interestingly, the measured charge density shows a proportional relation with the interface barrier, which is in contrast with the previous theories. On the basis of the results, a backflow-stuck charge model is proposed where the charge density is determined by the amount of backflow and the remaining stuck charges at separation. We also validated this model by comparing the theoretically predicted barrier and the extracted barrier from the temperature-dependent triboelectrification. The results soundly support that backflow-stuck charges determine the charge density at TE, where the interface barrier plays a key role. The model provides a new perspective of the charge transfer mechanism on the TE and can be generally applied to TE of conventional materials.

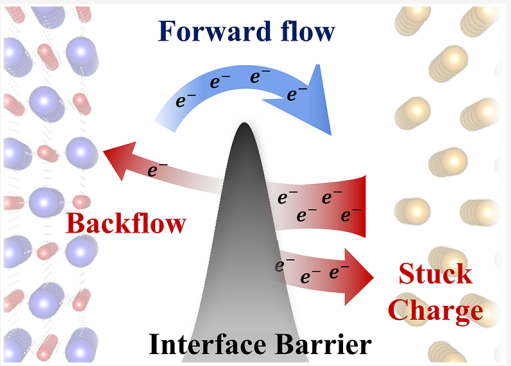

Triboelectrification (TE), the process of materials becoming electrically charged after contacting different materials, is a commonplace phenomenon that has been utilized for commercial applications (e.g., printing[1,2] and sensors[3−5]), while also being extensively investigated for self-powered electronics and energy harvesting systems.[6−14] Although this phenomenon has a long history of research that is becoming increasingly urgent in order to tackle practical energy problems, little is known about the associated material-dependent properties. The triboelectric series—the ranking of various materials according to their propensity to gain or lose electrons—was first published in 1757,[15] but understanding the mechanisms involved in this ranking has remained a long-standing and unresolved issue. One perspective proposed nearly a century ago is that this TE phenomenon appears simple, yet is actually rather baffling, and our understanding is still in the pioneering stage despite great efforts.[16] Since then, modern scientific techniques have been applied to understand this fundamental phenomenon for several generations; however, more puzzling behaviors continue to emerge in the process. As such, the perspective in this field is still baffling, and the understanding of the TE mechanism remains primitive.[17]

Because the triboelectric series is purely empirical,[18,19] it is thus highly dependent on material pairs (e.g., microstructure, composition, particle size, and surface configuration) and sensitive to experimental conditions (e.g., humidity, temperature, and loading stress/frequency). Moreover, tribocharging through contact-separation is a complex nonequilibrium process involving various scientific aspects such as electrostatics,[20,21] surface chemistry,[22,23] friction,[24] and stress−strain.[25] For these reasons, scientific progress toward defining the fundamental principle that underlies the ordering of the materials in the triboelectric series has been slow and remains largely unknown. Elucidating the fundamental principle will allow researchers to forecast the polarity of charges produced by TE, while also providing insights into design criteria for energy harvesting devices.[26−28]

In particular, there is little consensus on the theories surrounding TE in regard to charge transfer mechanisms or descriptive properties of materials to explain the ranking of the triboelectric series. TE between metals almost certainly involves electron transfer according to the difference in electronic work functions of the metals, which has been rigorously demonstrated in various studies.[29,30] On the other hand, for TE of insulating materials, it is still unclear whether the charged species that transfer from one material to another are electrons, ions, or charged materials (mass). For polymers, hydrophilicity and

Received: May 20, 2021
Accepted: July 6, 2021

https://doi.org/10.1021/acsenergylett.1c01019
ACS Energy Lett. 2021, 6, 2792−2799

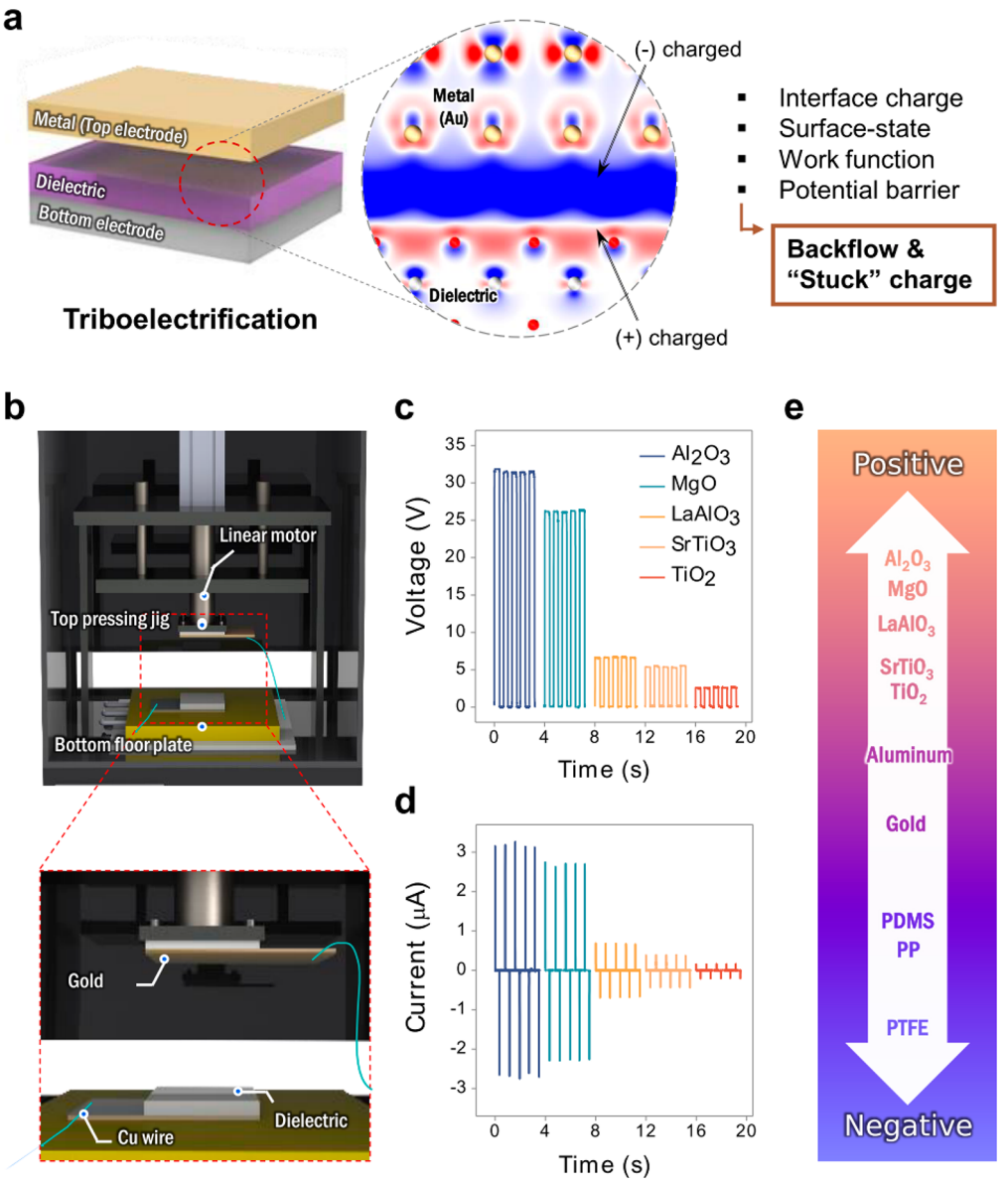

Figure 1. Triboelectrification of the Au-dielectric and triboelectric series. (a) Schematic of the metal-dielectric triboelectrification (TE) measuring device (triboelectric generator, TEG). The magnified interface is shown with a theoretical electronic configuration at the atomic scale. Four models were assessed to identify the mechanism of triboelectric charge transfer between a metal (Au) and five different inorganic dielectric materials (Al_2O_3, MgO, $LaAlO_3$, $SrTiO_3$, and TiO_2). A new perspective that combines electron backflow with "stuck" charges caused by interface potential barriers was thus proposed. (b) Schematic illustration of a pressing stage to measure triboelectric output. (c) Generated triboelectric signals of open-circuit voltage and (d) short-circuit current. (e) Triboelectric series including the representative inorganic dielectric materials investigated in this study, arranged according to the order of the generated triboelectric output.

Lewis basicity[31] have been proposed to determine the tribocharging series. Surprisingly, inorganic dielectric materials, which by definition contain a bandgap that regulates electron mobility, lie on both ends of the triboelectric series. In an effort to consistently examine TE for a number of common inorganic nonmetallic materials, Zou et al.[19] recently assesses nearly 30 materials and showed there is no clear correlation between dielectric constant and TE outputs. Instead, they claimed that the work function may be the descriptor for TE. However, only a limited number of work functions are presented, and as the authors stated, the defects (especially grain boundaries) can significantly modify the work functions, which is often hardly excluded from experimental studies. Therefore, a large part of TE in inorganic dielectrics still remains inconclusive.

Recently, the main triboelectric charged species generated on inorganic dielectric surfaces (SiO_2, Al_2O_3, and Si_3N_4) were identified as electrons by exploring the triboelectric charge decay under different temperatures at both the macroscale and the nanoscale, which was explained by the thermionic emission theory.[32,33] While it is convincing from experimental observations that electrons predominantly contribute to the TE in metal-dielectric or dielectric-dielectric interfaces, more questions remain: What is the qualitative description of how electrons are transferred? Which properties of materials or material pairs can be quantitatively ascribed to the tribocharge and explain the triboelectric ranking? To address these concerns, various plausible models for electron transfer have been suggested, such as the spatial charge redistribution

https://doi.org/10.1021/acsenergylett.1c01019
ACS Energy Lett. 2021, 6, 2792−2799

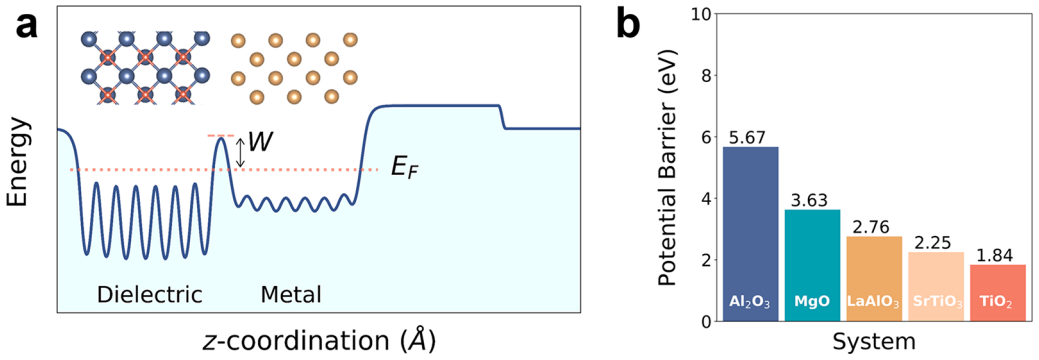

Figure 2. (a) **Schematic illustration of the previous interfacial potential barrier model of the Au-MgO system at an interface distance of 2.5 Å, showing the average electrostatic potential along the *z*-axis. (b) Calculated interface barriers of Au-dielectric systems at the equilibrium distance.**

model,[32,34,35] the surface state model,[36−38] the effective work function model,[39−42] and the interface potential barrier model.[32,43] However, none of these models comprehensively resolved the above questions due to various difficulties related to high-quality sample preparation to exclude mixed extrinsic effects and a lack of comprehensive coordination between quantitative calculations and measurements.

The main purpose of this study is to facilitate the establishment of an electron transfer mechanism and provide a quantitative understanding of the triboelectric series through analysis of experimental results and first-principles calculations performed on a series of Au-dielectric pairs under controlled conditions, as depicted in Figure 1a. The first-principles results are utilized to assess the previously proposed electron transfer mechanisms (i.e., charge redistribution, surface state, effective work function, and interface barrier models) in a metal-dielectric TE. Furthermore, we propose a backflow-stuck charge model that is based on the electron backflow emission, which is a key for determining the amount of "stuck" charges. In our backflow-stuck charge model, the electrostatic interface barrier between two materials determines the quantity of electronic backflow and stuck charges.

Material samples and experimental design were carefully chosen to obtain quantified intrinsic TE values. Figure 1b illustrates the contact-separation machine setup for TE experiments. A given dielectric single crystal wafer and the Au metal film were attached on the bottom floor plate and the top pressing jig, respectively, in a Faraday cage frame to block any external fields. During the up-and-down movement of the top jig, the two counterpart surfaces (metal-dielectric) undergo the contact-separation mode of TE. Sliding mode TE is excluded in this study because it includes more complex extrinsic factors such as shear stress and severe abrasion. Therefore, our experimental setup can be considered a contact electrification-based triboelectric generator (TEG). Further details are described in Supporting Information (SI) Methods 1. Figure 1c,d display the generated open-circuit voltage and the short-circuit current signals by the TEG, respectively (for the details see SI Methods 2). All triboelectric signals were measured after a stabilizing triboelectric process was maintained for a few seconds to achieve saturated TE.

Five types of inorganic dielectric single crystal materials (i.e., Al_2O_3, MgO, $LaAlO_3$, $SrTiO_3$, and TiO_2) generated distinctly different signals. For instance, the Au−Al_2O_3 TEG generates ∼32 V and ∼3 μA, whereas the Au-TiO_2 TEG produces ∼2.5 V and ∼100 nA. Note that we selected five inorganic dielectric materials that do not possess ferroelectric polarization or piezoelectric interference for this study. The choice of using single crystals is another important aspect because other effects from main defects, such as grain boundaries, must be avoided. Therefore, we selected commercially available oxide wafers with polished surfaces and identical thickness to control material conditions. As a counterpart triboelectric metal surface, Au film was utilized because it is chemically inert while also being triboelectrically neutral (positioned nearly in the middle of the triboelectric series, as shown in Figure 1e). Moreover, the energy states of the different crystal orientations of Au film are very similar, as shown in SI Note 1. Based on the measured triboelectric signals, the dielectric materials are arranged from the positive side of the triboelectric series in the following order: Al_2O_3 > MgO > $LaAlO_3$ > $SrTiO_3$ > TiO_2, as designated in Figure 1e.

Herein, four TE electron transfer mechanisms (I−IV) that are under debate in the literature are assessed using first-principles calculations combined with experimental results. The computational details can be found in the SI Methods 3 as well as in the SI Notes 2 and 3. The description of these models, namely (I) spatial charge redistribution, (II) surface state, (III) effective work function change, and (IV) interface potential barrier model, are presented in SI Note 5.

Based on our first-principles analysis for mechanisms, only interface potential barrier (IV) showed strong correlation with experimentally measured charge density and material-pair dependency; none of the other models successfully account for experimental observations. The detailed analysis for mechanisms (I−III) is presented in SI Note 5 and Figure S4.[44−48] The interface barrier (W) is defined as the difference between the maximum electrostatic potential of the interface and the Fermi level at equilibrium. Figure 2a schematically illustrates a planar electrostatic potential at contact (i.e., equilibrium), reflecting the change of the average potential along the axis perpendicular to the contact surface (z-axis). From the planar potential of Au-dielectric pairs (Figure S7), the density functional theory (DFT) calculated interface barriers were identified and are summarized in Figure 2b. It is noteworthy that the theoretical order of barrier heights clearly corresponds to the experimentally measured order of triboelectric output. Such a correlation seems to be a strange phenomenon because the previous interface potential barrier model qualitatively expected and suggested that a higher potential barrier restrains electron transfer across the interface, resulting in lower triboelectric signals.[49] Interestingly, however,

https://doi.org/10.1021/acsenergylett.1c01019
ACS Energy Lett. 2021, 6, 2792−2799

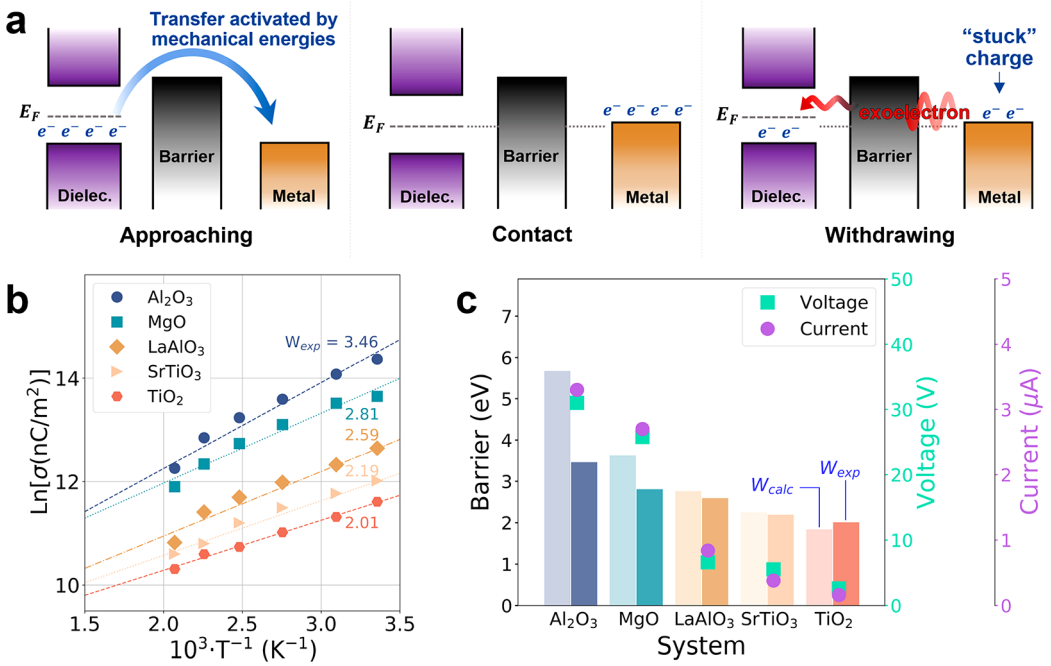

Figure 3. "Backflow-stuck charge" model and its validation. (a) "Backflow-stuck charge" model illustrated in the following three stages: (left) approaching, (middle) full contact, and (right) withdrawing. (b) Measured triboelectric charge density with increasing temperature for each Au-dielectric material system. Dashed lines are fitted to the equation in the main text, and the extracted barrier values from experiments are displayed. (c) Calculated and experimental interface potential barrier, also compared with the experimentally measured triboelectric voltage and current.

a positive relationship between the theoretical interface barrier and the experimental triboelectric output was observed from our quantitative first-principles DFT calculations, thus indicating a completely inverse tendency compared with the previous potential barrier model. Therefore, this paradoxical phenomenon shall be interpreted in greater detail below.

To understand how the interface potential barrier determines the output current and voltage, the process of electron transfer first needs to be considered. Here, the backflow-stuck charge model for TE during the contact-separation process is proposed with three stages of TE: (i) approaching, (ii) contact, and (iii) withdrawing.

As depicted in Figure 3a, the Fermi level of the dielectric material, which is usually more tribo-positive, is greater than the metal before contact.

(i) When the materials are "approaching" each other in close proximity, an electrostatic interface barrier emerges between them. The height of the interface barrier is different for dissimilar material pairs. Despite the existence of the barrier, electrons can easily be transported from the dielectric to the metal because the input mechanical energy during TE exceeds the energy to overcome the barrier. For our experimental conditions using a general TEG to evaluate a simple contact TE process with a normal force of 50 N, contact area of 100 mm^2 (= 0.5 MPa), and velocity of 0.1 m/s, we can estimate the maximum energy flux to be $\sim 10^4$ J/m^2s ($\sim 10^4$ eV/atom/s). Considering the mass ratio between the nucleus and electron ($\sim 10^3$ to 10^4:1), the scale of energy flux on an electron is far beyond the thermal energy at room temperature ($k_bT \approx 0.02$ eV), and it can generate hot electrons that overcome the interface potential barrier. Given the scale of these forces, the input energy is also sufficiently higher than the energy required to activate electron transfer from one surface to another by activating various mechanisms such as phonon-drag, flexoelectricity, and frictional heat. Specifically, phonons generated by lattice vibrations can interact with electrons, where it has been shown that the kinetic energy of electrons can drastically increase via the phonon-drag effect.[50,51] Furthermore, it is also plausible for electron transfer to occur via atomic bond breaking,[52,53] strain gradient-induced electrical polarization (i.e., flexoelectricity),[45] field emission (i.e., quantum tunneling),[39,54] or coupled effects of the listed mechanism (I–IV). In short, initial "forward-flow" occurs, regardless of the mechanism because there is more than sufficient driving force from the mechanical contact.

(ii) At the "contact" stage ($d = d_{eq}$), the Fermi levels of each material are aligned due to charge balance at the interface. Electrons from the dielectric material flow into the metal counterpart until equilibrium is reached between the two materials. Excess electrons reside on the metal surface while electrons are depleted on the dielectric surface.

(iii) As the two materials are "withdrawing" from each other, the extra charges on the metal surface will experience a thermodynamic driving force for "backflow" to return to the original electronic state without interface. At this stage, there is no direct influence from mechanical force (i.e., insufficient energy to activate electron transfer, unlike in stage (i)), but the lattice vibration or deformation originating from the detachment of two surfaces allows kinetic activation for backflow emission. The electrons excited by nonstationary external effects such as lattice vibrations, so-called exoelectrons,[55] can tunnel with a certain probability, where the probability is primarily determined by the magnitude of the potential

https://doi.org/10.1021/acsenergylett.1c01019
ACS Energy Lett. 2021, 6, 2792−2799

barrier. The kinetic energy of exoelectrons on the metal surface range from 0.0 to 1.5 eV due to the lattice vibration.[56] These electrons with kinetic energy possess a certain probability to flow back from the metal to the dielectric material by quantum tunneling, thus resulting in the rest of the electrons on the metal surface remaining as "stuck" charges, which corresponds to the experimental charge density.

Up to this point, we have corroborated the backflow-stuck charge model for TE, which depends on the barriers of metal-dielectric systems. It is worth noting that the concept of backflow and "stuck" charges was taken into consideration in previous studies;[29,52,57,58] however, conventional theories on the mechanism of TE focused on the correlation only between forward-flow and tribo-charges, whereas the key factor determining the tribo-charges is indeed the stuck charge associated with backflow. Using our new perspective, the model further clarifies some previously unclear observations in TE phenomena. In this work and a previous theoretical study,[58] a large discrepancy between calculated and measured triboelectric charge density levels was shown, with approximately 4−5 orders of magnitude difference (as in Figure 2b). The measured charge density is far less than the thermal equilibrium charge density, which indicates that the charges are not entirely transferred; it is plausible that only stuck charges are significantly involved in triboelectric signal generation in experimental measurements.

In recent study of temporally resolved signal analysis, it was discovered that there were asymmetric wave forms of voltage signals at the separation state.[59] Intriguingly, this observation evidently showed that transferred electrons (from dielectric to metal) at the contact state can flow back considerably to the initial surface (from metal to dielectric). Furthermore, it is well-known that triboelectric generating signals from initial contacts do not agree with the final saturated triboelectric output that should be obtained after repeating contact-separation cycles several times, called a stabilizing triboelectric process (in fact, many studies about triboelectric energy harvesting inevitably undergo such a process to stabilized and maximized TEG performance). If triboelectric charging is dominated by forward-flow, it is difficult to physically understand that a considerable amount of contact time is required for saturated TE, because the driving force of forward-flow at the contact state is already much greater than the energy needed for electron transfer, as mentioned earlier. In contrast, this behavior can easily be explained by the backflow-stuck charge model; because of the existence of the interface barrier and the finite probability of tunneling, stuck charges (remaining electrons after backflow) accumulate gradually while the contact/separation cycles are repeated and eventually reach saturation. Therefore, these universal observations in TE support the validity of the backflow-stuck charge model.

To further verify the model and electrostatic barrier dependence obtained from theoretical calculations, we extracted barrier values from variable temperature experiments. Whereas forward-flow is nearly independent of temperature since there is always sufficient energy for electron transfer, the number of stuck charges should decrease as the temperature increases because thermal energy promotes the backflow of electrons with thermionic emission.[60,61] The charge density of metal-dielectric systems at elevated temperature (298−523 K) was experimentally measured (Figure 3b and Figure S8). If the process is regulated by the interface barrier, then the temperature-dependent kinetics should follow an Arrhenius relationship. Thus, the charge density, σ, is expressed as

$$\sigma = \sigma_0\left(1 - A_0 \exp\left(-\frac{W}{k_b T}\right)\right) \quad (1)$$

where σ_0 is the ideal charge density that is transferrable without backflow. The term $\exp\left(-\frac{W}{k_b T}\right)$ is the Boltzmann probability of an electron overcoming the potential barrier, W (i.e., backflow), where k_b and T are the Boltzmann constant and the temperature, respectively. The A_0 is a dimensionless pre-exponential factor expressed as $A_0 = \omega_0 t_s$, where ω_0 is an attempt frequency and t_s is accumulated contact/separation time to reach tribo-charging saturation. The ω_0 was set at a constant value of equilibrium phonon frequency, 10 THz, which is the upper bound of the equilibrium phonon frequency range for crystals (1−10 THz).[62] The t_s was set to 5 s based on our experimental results. Since $\exp\left(-\frac{W}{k_b T}\right) \ll 1$ at the temperature range used in this study, the above expression can be rewritten with a first-order approximation as

$$\ln(\sigma) = \frac{A_0 W}{k_b}\frac{1}{T} + \text{const} \quad (2)$$

The $A_0 W/k_b$ term can be expressed as the slope of $\ln(\sigma)$ as a function of T^{-1} from eq 2, as shown in Figure 3b. The experimentally determined barriers (W_{exp}) are in the range of 2.01 to 3.46 eV depending on the type of material. The relative order of the barriers extracted from the experiments corresponds well to that of the DFT calculated barriers (W_{calc}) of Al_2O_3 > MgO > $LaAlO_3$ > $SrTiO_3$ > TiO_2. In Figure 3c, W_{calc} and W_{exp} are plotted for comparison, as well as the experimentally measured triboelectric output in order to visualize the relationship between them, resulting in well-matched tendencies. Comparison of the absolute values of the theoretical and experimental potential barriers indicates that the W_{exp} and W_{calc} are similar, with some discrepancies that arise because the theoretically calculated barrier is based on the thermodynamic equilibrium condition at steady-state, whereas it is difficult to achieve this in the experimental system; thus, a discrepancy in the absolute values of W_{calc} and W_{exp} is expected. Furthermore, the nonequilibrium state may act as an additional driving force, causing an effective lowering of the barrier that electrons experience. Especially for Au−Al_2O_3, hydrogen present on the surface might impose easier electron transfer via material transport (SI Note 2);[20] notwithstanding, the fact that the tendencies are the same does not change. This agreement between W_{calc} and W_{exp} provides a robust support for the backflow-stuck charge model.

In Figure 3c, the triboelectric voltage and current signals decrease exponentially as the barriers decrease, implying that the TE output is expressed in an exponential function that includes the interface potential barrier. To extend our approach to exploit the quantum-tunneling effect, a numerical calculation for the barrier dependency of tunneling probability was performed. As shown in SI Note 6, the tunneling effect is a barrier-dependent exponential function, which explains the nonlinear and positive relationship between the potential barrier and the triboelectric voltage/current output, further supporting the validity of the backflow-stuck charge model.

https://doi.org/10.1021/acsenergylett.1c01019
ACS Energy Lett. 2021, 6, 2792−2799

In conclusion, a straightforward design of TE for a metal-dielectric series has been investigated to understand the most dominant electron transfer mechanism in TE—both qualitatively and quantitatively—to establish an advanced triboelectric charging model. By comparing experimental measurements with first-principles calculations, we examined four types of electron transfer mechanisms based on the: (I) simple charge redistribution model, (II) surface bandgap state model, (III) work function change model, and (IV) interface potential barrier model. It is clear that the triboelectric voltage/current output exhibits a positive relationship with the interface barrier, whereas the other mechanisms ultimately provided either an insignificant contribution to triboelectric charging or an unclear relationship with the barrier. In contrast to previous theories mostly focusing on the forward-flow of electrons just after mechanical contact, our results advocate that the stuck charges (i.e., the charges that survived from the backflow of electrons just before subsequent separation) is the foundation of tribo-charging. To elaborate these points, a backflow-stuck charge model was proposed: electrons can always allowedly flow forward upon mechanical contact due to sufficient driving force, but the net triboelectric charge density is determined by the amount of backflow and the remaining stuck charge at the interface barrier. The agreement between the theoretically calculated barrier and the experimentally fitted barrier from the temperature-dependent results suggests that the interface barrier plays a significant role in the positive relationship with final tribo-charging.

Finally, analysis of quantum tunneling probability confirmed electron backflow emission, as the exponentially positive relationship with the barrier and the experimental TE output was verified. Our model refines the mechanism of TE, providing information for rethinking the mechanisms involved in the ranking of the conventional triboelectric series. Although we have used the single crystal dielectric ceramics in this study to exclude complex artifacts from grain boundary defects, there are no theoretical problems in applying this advanced model to polycrystalline dielectric materials. Moreover, the backflow and stuck charge model can be also adopted to metal−metal pair or dielectric−dielectric pair systems as well as metal−dielectric systems. In metal−metal triboelectric pair systems, this model might be less important due to low potential barrier in triboelectric charging. In dielectric−dielectric pair systems, it should be noted that ion transfers or mass transfers become more dominant than electron transfers. Therefore, the backflow and stuck charge model can be adapted to other systems, although it is also more complicated and possibly modified by other charge types. In summary, the barrier-dependent stuck charge model unveiled in this study will help understand tribo-charging phenomena and the triboelectric series of dielectric materials, which can shed a light on evaluating tribo-electrification for metal-dielectric pairs as well as for other material pairs, which can aid the development of improved triboelectric devices such as sensors and renewable energy applications in the future.

■ ASSOCIATED CONTENT

Supporting Information

The Supporting Information is available free of charge at https://pubs.acs.org/doi/10.1021/acsenergylett.1c01019.

Materials, experimental and computational methodologies, and additional theoretical analysis, which consists of Methods 1−3, Notes 1−6, Table S1, and Figures S1−S10 (PDF)

■ AUTHOR INFORMATION

Corresponding Authors

Chang Kyu Jeong − *Division of Advanced Materials Engineering, Jeonbuk National University, Jeonju, Jeollabuk-do 54896, Republic of Korea; Department of Energy Storage/Conversion Engineering of Graduate School & Hydrogen and Fuel Cell Research Center, Jeonbuk National University, Jeonju, Jeollabuk-do 54896, Republic of Korea;* orcid.org/0000-0001-5843-7609; Email: ckyu@jbnu.ac.kr

Sung Beom Cho − *Convergence Technology Division, Korea Institute of Ceramic Engineering and Technology (KICET), Jinju, Gyeongsangnam-do 52851, Republic of Korea;* Email: csb@kicet.re.kr

Authors

Hyunseok Ko − *Research Institute of Advanced Materials, Seoul National University, Seoul 08826, Republic of Korea; Convergence Technology Division, Korea Institute of Ceramic Engineering and Technology (KICET), Jinju, Gyeongsangnam-do 52851, Republic of Korea*

Yeong-won Lim − *Division of Advanced Materials Engineering, Jeonbuk National University, Jeonju, Jeollabuk-do 54896, Republic of Korea; Department of Energy Storage/Conversion Engineering of Graduate School & Hydrogen and Fuel Cell Research Center, Jeonbuk National University, Jeonju, Jeollabuk-do 54896, Republic of Korea*

Seungwu Han − *Research Institute of Advanced Materials, Seoul National University, Seoul 08826, Republic of Korea; Department of Materials Science and Engineering, Seoul National University, Seoul 08826, Republic of Korea;* orcid.org/0000-0003-3958-0922

Complete contact information is available at: https://pubs.acs.org/10.1021/acsenergylett.1c01019

Author Contributions

‖H.K. and Y.L. contributed equally to this work.

Notes

The authors declare no competing financial interest.

■ ACKNOWLEDGMENTS

This research was supported by the National Research Foundation of Korea (NRF-2019R1C1C1002571, 2019R1F1A1058554). We gratefully acknowledge support from the Ministry of Science and ICT (NRF-2020M3H4A3081867) and the *i*-ceramic project from the Ministry of Trade, Industry & Energy (20004367). Computations were carried out using resources from the Korea Supercomputing Center (KSC-2020-CRE-0023).

■ REFERENCES

(1) Seol, M.-L.; Han, J.-W.; Moon, D.-I.; Yoon, K. J.; Hwang, C. S.; Meyyappan, M. All-printed triboelectric nanogenerator. *Nano Energy* **2018**, *44*, 82−88.

(2) Chen, B.; Yang, N.; Jiang, Q.; Chen, W.; Yang, Y. Transparent triboelectric nanogenerator-induced high voltage pulsed electric field for a self-powered handheld printer. *Nano Energy* **2018**, *44*, 468−475.

(3) Wang, H.; Xiang, Z.; Giorgia, P.; Mu, X.; Yang, Y.; Wang, Z. L.; Lee, C. Triboelectric liquid volume sensor for self-powered lab-on-chip applications. *Nano Energy* **2016**, *23*, 80−88.

(4) Zhao, X.; Chen, B.; Wei, G.; Wu, J. M.; Han, W.; Yang, Y. Polyimide/Graphene Nanocomposite Foam-Based Wind-Driven Triboelectric Nanogenerator for Self-Powered Pressure Sensor. *Advanced Materials Technologies* **2019**, *4* (5), 1800723.
(5) Chen, X.; Gao, L.; Chen, J.; Lu, S.; Zhou, H.; Wang, T.; Wang, A.; Zhang, Z.; Guo, S.; Mu, X.; Wang, Z. L.; Yang, Y. A chaotic pendulum triboelectric-electromagnetic hybridized nanogenerator for wave energy scavenging and self-powered wireless sensing system. *Nano Energy* **2020**, *69*, 104440.
(6) Wang, S. H.; Lin, L.; Wang, Z. L. Nanoscale Triboelectric-Effect-Enabled Energy Conversion for Sustainably Powering Portable Electronics. *Nano Lett.* **2012**, *12*, 6339.
(7) Lee, B.-Y.; Kim, D. H.; Park, J.; Park, K.-I.; Lee, K. J.; Jeong, C. K. Modulation of surface physics and chemistry in triboelectric energy harvesting technologies. *Sci. Technol. Adv. Mater.* **2019**, *20* (1), 758−773.
(8) Chun, S.; Pang, C.; Cho, S. B. A Micropillar-Assisted Versatile Strategy for Highly Sensitive and Efficient Triboelectric Energy Generation under In-Plane Stimuli. *Adv. Mater.* **2020**, *32* (2), 1905539.
(9) Ahmed, A.; Hassan, I.; Helal, A. S.; Sencadas, V.; Radhi, A.; Jeong, C. K.; El-Kady, M. F. Triboelectric Nanogenerator versus Piezoelectric Generator at Low Frequency (<4 Hz): A Quantitative Comparison. *iScience* **2020**, *23* (7), 101286.
(10) Ahmed, A.; Hassan, I.; El-Kady, M. F.; Radhi, A.; Jeong, C. K.; Selvaganapathy, P. R.; Zu, J.; Ren, S.; Wang, Q.; Kaner, R. B. Integrated Triboelectric Nanogenerators in the Era of the Internet of Things. *Adv. Sci.* **2019**, *6* (24), 1802230.
(11) Yang, Y.; Zhang, H.; Wang, Z. L. Direct-Current Triboelectric Generator. *Adv. Funct. Mater.* **2014**, *24* (24), 3745−3750.
(12) Zhao, K.; Yang, Y.; Liu, X.; Wang, Z. L. Triboelectrification-Enabled Self-Charging Lithium-Ion Batteries. *Adv. Energy Mater.* **2017**, *7* (21), 1700103.
(13) Su, Y.; Yang, Y.; Zhong, X.; Zhang, H.; Wu, Z.; Jiang, Y.; Wang, Z. L. Fully Enclosed Cylindrical Single-Electrode-Based Triboelectric Nanogenerator. *ACS Appl. Mater. Interfaces* **2014**, *6* (1), 553−559.
(14) Quan, T.; Wang, Z. L.; Yang, Y. A Shared-Electrode-Based Hybridized Electromagnetic-Triboelectric Nanogenerator. *ACS Appl. Mater. Interfaces* **2016**, *8* (30), 19573−19578.
(15) Wilcke, J. C. Disputatio Physica Experimentalis, de Electricitatibus Contrariis [Latin]. Ph.D. Thesis, Rostochii: Typis Joannis Jacobi Adleri, 1757.
(16) Shaw, P. E. The Electrical Charges from Like Solids. *Nature* **1926**, *118* (2975), 659−660.
(17) Lacks, D. J.; Shinbrot, T. Long-standing and unresolved issues in triboelectric charging. *Nat. Rev. Chem.* **2019**, *3* (8), 465−476.
(18) Zou, H.; Zhang, Y.; Guo, L.; Wang, P.; He, X.; Dai, G.; Zheng, H.; Chen, C.; Wang, A. C.; Xu, C.; Wang, Z. L. Quantifying the triboelectric series. *Nat. Commun.* **2019**, *10* (1), 1427.
(19) Zou, H.; Guo, L.; Xue, H.; Zhang, Y.; Shen, X.; Liu, X.; Wang, P.; He, X.; Dai, G.; Jiang, P.; Zheng, H.; Zhang, B.; Xu, C.; Wang, Z. L. Quantifying and understanding the triboelectric series of inorganic non-metallic materials. *Nat. Commun.* **2020**, *11* (1), 2093.
(20) McCarty, L. S.; Whitesides, G. M. Electrostatic Charging Due to Separation of Ions at Interfaces: Contact Electrification of Ionic Electrets. *Angew. Chem., Int. Ed.* **2008**, *47* (12), 2188−2207.
(21) Wang, Z. L. On Maxwell's displacement current for energy and sensors: the origin of nanogenerators. *Mater. Today* **2017**, *20* (2), 74−82.
(22) Shin, S.-H.; Bae, Y. E.; Moon, H. K.; Kim, J.; Choi, S.-H.; Kim, Y.; Yoon, H. J.; Lee, M. H.; Nah, J. Formation of Triboelectric Series via Atomic-Level Surface Functionalization for Triboelectric Energy Harvesting. *ACS Nano* **2017**, *11* (6), 6131−6138.
(23) Feng, Y.; Zheng, Y.; Ma, S.; Wang, D.; Zhou, F.; Liu, W. High output polypropylene nanowire array triboelectric nanogenerator through surface structural control and chemical modification. *Nano Energy* **2016**, *19*, 48−57.
(24) Knorr, N. Squeezing out hydrated protons: low-frictional-energy triboelectric insulator charging on a microscopic scale. *AIP Adv.* **2011**, *1* (2), 022119.
(25) Pan, S.; Zhang, Z. Fundamental theories and basic principles of triboelectric effect: A review. *Friction* **2019**, *7* (1), 2−17.
(26) Chen, X.; Ren, Z.; Han, M.; Wan, J.; Zhang, H. Hybrid energy cells based on triboelectric nanogenerator: From principle to system. *Nano Energy* **2020**, *75*, 104980.
(27) Quan, T.; Yang, Y. Fully enclosed hybrid electromagnetic−triboelectric nanogenerator to scavenge vibrational energy. *Nano Res.* **2016**, *9* (8), 2226−2233.
(28) Quan, T.; Wu, Y.; Yang, Y. Hybrid electromagnetic−triboelectric nanogenerator for harvesting vibration energy. *Nano Res.* **2015**, *8* (10), 3272−3280.
(29) Lowell, J.; Rose-Innes, A. C. Contact electrification. *Adv. Phys.* **1980**, *29* (6), 947−1023.
(30) Pai, D. M.; Springett, B. E. Physics of electrophotography. *Rev. Mod. Phys.* **1993**, *65* (1), 163−211.
(31) Zhang, X.; Chen, L.; Jiang, Y.; Lim, W.; Soh, S. Rationalizing the Triboelectric Series of Polymers. *Chem. Mater.* **2019**, *31* (5), 1473−1478.
(32) Xu, C.; Zi, Y.; Wang, A. C.; Zou, H.; Dai, Y.; He, X.; Wang, P.; Wang, Y.-C.; Feng, P.; Li, D.; Wang, Z. L. On the Electron-Transfer Mechanism in the Contact-Electrification Effect. *Adv. Mater.* **2018**, *30* (15), 1706790.
(33) Lin, S.; Xu, L.; Xu, C.; Chen, X.; Wang, A. C.; Zhang, B.; Lin, P.; Yang, Y.; Zhao, H.; Wang, Z. L. Electron Transfer in Nanoscale Contact Electrification: Effect of Temperature in the Metal−Dielectric Case. *Adv. Mater.* **2019**, *31* (17), 1808197.
(34) Fu, Q.; Wagner, T. Interaction of nanostructured metal overlayers with oxide surfaces. *Surf. Sci. Rep.* **2007**, *62* (11), 431−498.
(35) Cho, S. B.; Yun, K.-H.; Yoo, D. S.; Ahn, K.; Chung, Y.-C. Work function tuning of an ultrathin MgO film on an Ag substrate by generating oxygen impurities at the interface. *Thin Solid Films* **2013**, *544*, 541−544.
(36) Ernst, L. Optical spectroscopy of surface states on NaCl and KCl crystals and its relation to contact charging. *Solid State Commun.* **1976**, *19* (4), 311−314.
(37) Kittaka, S.; Murata, Y. Photoelectric Emission and Contact Charging of Vacuum-UV Irradiated Polymers. *Jpn. J. Appl. Phys.* **1979**, *18* (3), 515−521.
(38) Lacks, D. J.; Duff, N.; Kumar, S. K. Nonequilibrium Accumulation of Surface Species and Triboelectric Charging in Single Component Particulate Systems. *Phys. Rev. Lett.* **2008**, *100* (18), 188305.
(39) Chiu, F.-C. A Review on Conduction Mechanisms in Dielectric Films. *Adv. Mater. Sci. Eng.* **2014**, *2014*, 578168.
(40) Franciosi, A.; Van de Walle, C. G. Heterojunction band offset engineering. *Surf. Sci. Rep.* **1996**, *25* (1), 1−140.
(41) Yeo, Y.-C.; King, T.-J.; Hu, C. Metal-dielectric band alignment and its implications for metal gate complementary metal-oxide-semiconductor technology. *J. Appl. Phys.* **2002**, *92* (12), 7266−7271.
(42) Zhong, Z.; Hansmann, P. Band Alignment and Charge Transfer in Complex Oxide Interfaces. *Phys. Rev. X* **2017**, *7* (1), 011023.
(43) Wu, J.; Wang, X.; Li, H.; Wang, F.; Yang, W.; Hu, Y. Insights into the mechanism of metal-polymer contact electrification for triboelectric nanogenerator via first-principles investigations. *Nano Energy* **2018**, *48*, 607−616.
(44) Antony, A. C.; Thelen, D.; Zhelev, N.; Adib, K.; Manley, R. G. Electronic charge transfer during metal/SiO2 contact: Insight from density functional theory. *J. Appl. Phys.* **2021**, *129* (6), 065304.
(45) Mizzi, C. A.; Lin, A. Y. W.; Marks, L. D. Does Flexoelectricity Drive Triboelectricity? *Phys. Rev. Lett.* **2019**, *123* (11), 116103.
(46) Chen, L.; Shi, Q.; Sun, Y.; Nguyen, T.; Lee, C.; Soh, S. Controlling Surface Charge Generated by Contact Electrification: Strategies and Applications. *Adv. Mater.* **2018**, *30* (47), 1802405.
(47) Fatti, G.; Righi, M. C.; Dini, D.; Ciniero, A. Ab Initio Study of Polytetrafluoroethylene Defluorination for Tribocharging Applications. *ACS Appl. Polym. Mater.* **2020**, *2* (11), 5129−5134.
(48) Zhang, Y.; Shao, T. Effect of contact deformation on contact electrification: a first-principles calculation. *J. Phys. D: Appl. Phys.* **2013**, *46* (23), 235304.

https://doi.org/10.1021/acsenergylett.1c01019
ACS Energy Lett. 2021, 6, 2792−2799

(49) Willatzen, M.; Wang, Z. L. Contact Electrification by Quantum-Mechanical Tunneling. *Research* **2019**, *2019*, 11.
(50) Zhou, J.; Liao, B.; Qiu, B.; Huberman, S.; Esfarjani, K.; Dresselhaus, M. S.; Chen, G. Ab initio optimization of phonon drag effect for lower-temperature thermoelectric energy conversion. *Proc. Natl. Acad. Sci. U. S. A.* **2015**, *112* (48), 14777−14782.
(51) Titov, O. Y.; Salazar Laureles, J. L.; Gurevich, Y. G. Hot phonons and electrons in semiconductors. *Superf. y Vacio* **2015**, *28*, 33−39.
(52) Lee, L.-H. Dual mechanism for metal-polymer contact electrification. *J. Electrost.* **1994**, *32* (1), 1−29.
(53) Baytekin, H. T.; Patashinski, A. Z.; Branicki, M.; Baytekin, B.; Soh, S.; Grzybowski, B. A. The Mosaic of Surface Charge in Contact Electrification. *Science* **2011**, *333* (6040), 308−312.
(54) Alicki, R.; Jenkins, A. Quantum Theory of Triboelectricity. *Phys. Rev. Lett.* **2020**, *125* (18), 186101.
(55) White, J. D.; Chen, J.; Matsiev, D.; Auerbach, D. J.; Wodtke, A. M. Conversion of large-amplitude vibration to electron excitation at a metal surface. *Nature* **2005**, *433* (7025), 503−505.
(56) LaRue, J.; Schäfer, T.; Matsiev, D.; Velarde, L.; Nahler, N. H.; Auerbach, D. J.; Wodtke, A. M. Vibrationally promoted electron emission at a metal surface: electron kinetic energy distributions. *Phys. Chem. Chem. Phys.* **2011**, *13* (1), 97−99.
(57) Lacks, D. J.; Mohan Sankaran, R. Contact electrification of insulating materials. *J. Phys. D: Appl. Phys.* **2011**, *44* (45), 453001.
(58) Shen, X.; Wang, A. E.; Sankaran, R. M.; Lacks, D. J. First-principles calculation of contact electrification and validation by experiment. *J. Electrost.* **2016**, *82*, 11−16.
(59) Musa, U. G.; Cezan, S. D.; Baytekin, B.; Baytekin, H. T. The Charging Events in Contact-Separation Electrification. *Sci. Rep.* **2018**, *8* (1), 2472.
(60) Xu, C.; Zhang, B.; Wang, A. C.; Cai, W.; Zi, Y.; Feng, P.; Wang, Z. L. Effects of Metal Work Function and Contact Potential Difference on Electron Thermionic Emission in Contact Electrification. *Adv. Funct. Mater.* **2019**, *29* (29), 1903142.
(61) Xia, X.; Wang, H.; Guo, H.; Xu, C.; Zi, Y. On the material-dependent charge transfer mechanism of the contact electrification. *Nano Energy* **2020**, *78*, 105343.
(62) Reed, E. J.; Armstrong, M. R.; Kim, K.; Soljačić, M.; Gee, R.; Glownia, J. H.; Joannopoulos, J. D. Terahertz radiation from shocked materials. *Mater. Today* **2007**, *10* (7), 44−50.

https://doi.org/10.1021/acsenergylett.1c01019
ACS Energy Lett. 2021, 6, 2792−2799